JACS
JOURNAL OF THE AMERICAN CHEMICAL SOCIETY

ARTICLE

pubs.acs.org/JACS

Electrochemistry and Electrogenerated Chemiluminescence of a Spirobifluorene-Based Donor (Triphenylamine)−Acceptor (2,1,3-Benzothiadiazole) Molecule and Its Organic Nanoparticles

Khalid M. Omer,[†] Sung-Yu Ku,[†,‡] Jian-Zhang Cheng,[‡] Shu-Hua Chou,[‡] Ken-Tsung Wong,*[,‡] and Allen J. Bard*[,†]

[†]Center for Electrochemistry, Department of Chemistry and Biochemistry, and Center for Nano-and Molecular Science and Technology, University of Texas at Austin, Austin, Texas 78712, United States

[‡]Department of Chemistry, National Taiwan University, 106 Taipei, Taiwan

Supporting Information

ABSTRACT: A new D−A−π−A−D molecule (Spiro-BTA) containing two 2,1,3-benzothiadiazole (BTA) as the acceptor (A) and triphenylamine as the donor (D) bridged by a spirobifluorene moiety has been synthesized. The novel D−A molecule shows intense red emission (612 nm) with a high PL quantum yield (Φ_{PL} = 0.51) in a solid film. A cyclic voltammogram of Spiro-BTA in 1:2 MeCN:benzene/0.1 M Bu_4NPF_6 shows two reversible oxidation waves and one reversible reduction wave. The first oxidation wave and reduction wave were assigned as two successive electron transfer peaks separated by ~50 mV related to the oxidation of the two noninteracting donors and the reduction of the two noninteracting acceptors, respectively. Electrogenerated chemiluminescence (ECL) of Spiro-BTA upon cyclic oxidation and reduction in MeCN:benzene 1:2 shows a very bright and stable red emission that could be seen in a well-lit room. Using a reprecipitation method, well-dispersed organic nanoparticles (NPs) of the Spiro-BTA were prepared in aqueous solution. The nanoparticles were analyzed by dynamic light scattering (DLS) and scanning electron microscopy (SEM), yielding a NP size (without surfactant) of 130 ± 20 nm, while with surfactant, 100 ± 20 nm. Bathochromic shifts of absorption spectra (~16 ± 2 nm), as compared to that of the dissolved Spiro-BTA in THF, were observed for both NPs in water and as a thin film. While blue shifts (14 ± 2 nm) were observed for the photoluminescence (PL). The PL intensity of the Spiro-BTA nanoparticles was slightly enhanced (Φ_{PL} of nanoparticles in water = 48%) over that of the dissolved Spiro-BTA in THF. The ECL of the organic Spiro-BTA nanoparticles in aqueous solution could be observed upon oxidation with tri-*n*-propylamine as a coreactant.

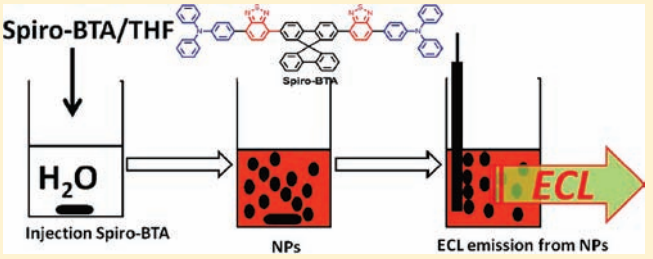

INTRODUCTION

We report the synthesis, spectroscopic and electrochemical characterization, as well as the electrogenerated chemiluminescence (ECL) of a new highly fluorescent molecule (Spiro-BTA) (structure shown in Scheme 1). Spiro-BTA is a C_2-symmetric donor−acceptor (DA) compound, consisting of spirobifluorene as the π-bridge core connected to two 2,1,3-benzothiadiazole (BTA) units as the acceptors (A) and end-capped with triphenylamines as the donors (D), with the overall structure D−A−π−A−D (see Scheme 1). There have been a number of studies of the electrochemical, spectroscopic, and ECL behavior of DA molecules.[1] While this paper considers analogous studies of this species in nonaqueous solutions, in addition, well-dispersed organic nanoparticles (NPs) with a narrow size distribution have been prepared in aqueous solution using a reprecipitation method.[3] The Spiro-BTA NPs in aqueous solution show enhanced fluorescence emission over the fluorescence in organic solution. Particularly interesting, a strong enhancement of the emission was observed by using surfactant to stabilize the Spiro-BTA NPs and produce smaller particle sizes. More remarkably, those particles can produce ECL emission after reacting with tripropylamine as a coreactant. Such observation may lead to important applications of using ECL of organic NPs in aqueous media as the emissive tag for the analysis of biologically interesting molecules.

The electrochemical and emission properties of organic NPs have been the subject of relatively few studies compared to inorganic NPs. For inorganic materials the physical and chemical properties observed in the corresponding bulk forms are very different when the particle size is reduced to the nanometer regime. The size effect of the properties of organic NPs is not expected to produce large changes in characteristics compared to the bulk crystal, because electrons are largely confined within

Received: January 4, 2011
Published: March 17, 2011

dx.doi.org/10.1021/ja2000825 | J. Am. Chem. Soc. 2011, 133, 5492–5499

Scheme 1. Synthetic Route to Spiro-BTA

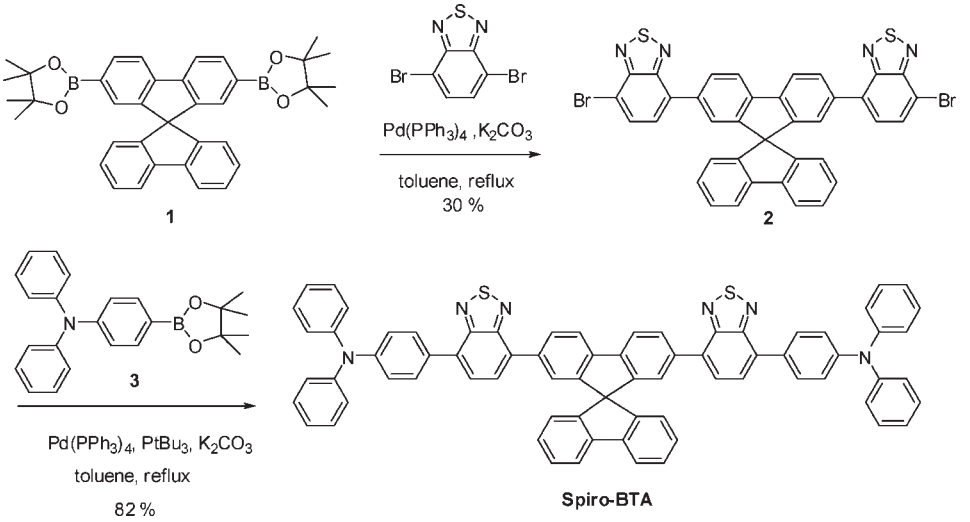

single molecules and do not delocalize or transfer over nanometer and micrometer domains.[2] Inorganic NPs have been suggested as biological fluorescent labels, but they are difficult to functionalize on a specific site and tend to be toxic and unstable under intense radiation. In contrast, organic molecules have the advantage of being easily functionalized with versatile synthetic strategies and, in addition, the possibility of tailoring the electronic and optical properties of organic molecules to fit a desired application. In principle, organic NPs might have practical applications because their fluorescence spans a wide wavelength region. The tailor-made molecular design strategy has triggered recent research interests in organic NPs generated from small organic molecules.[3] Because of the very small background light in the ECL technique, the ECL of organic NP labels in aqueous solution has potential applications in the future, for example, in bioanalytical methods. We recently reported ECL for organic NPs from the well-known ECL emitters 9,10-diphenylanthracene (DPA) and rubrene in aqueous media.[4] In addition, the ECL from nanobelts spontaneously formed from ionic metallic complexes with organic ligands dispersed in water has also been observed.[5] In these earlier works, control of the particle size of organic NPs was the main challenge, since the larger the particles, the smaller the diffusion coefficient and the weaker the ECL. However, the synthesis and control of the size and shape of organic nanoparticles are not as straightforward as the inorganic counterparts. A small diffusion coefficient is one of the crucial hurdles in electrochemical measurements of organic NPs and is still an issue that requires further study.

EXPERIMENTAL SECTION

Synthesis of Spiro-BTA. $Pd(PPh_3)_4$ (81 mg, 0.07 mmol), **2**[1c] (507 mg, 0.68 mmol), and *N*,*N*-diphenyl-4-(4,4,5,5-tetramethyl-1,3,2-dioxaborolan-2-yl)aniline (**3**)[6] (780 mg, 2.10 mmol) were added to a 50-mL two-neck flask with a septum. The flask was evacuated and backfilled with argon. Toluene (10 mL), P^tBu_3 (1.2 mL, 0.07 mmol, 0.05 M in toluene) and K_2CO_3 (2.7 mL, 1.0 M, 2.72 mmol) were added in order by a syringe at room temperature. The reaction mixture was heated at 110 °C for 72 h. The reaction mixture was allowed to cool to room temperature, water (30 mL) was added, and the mixture was extracted with CH_2Cl_2 (40 mL × 3). The combined organic solution was dried over $MgSO_4$ and concentrated in vacuum. Spiro-BTA (600 mg, 82% yield) was purified by chromatography with silica gel ($CHCl_3$:hexane: toluene 1:2:1): T_g 274 °C (DSC); mp >500 °C (DSC); ^{1}H NMR ($CDCl_3$, 400 MHz) δ 8.21 (d, J = 8.0, 2H), 8.09 (d, J = 8.0 Hz, 2H), 7.87 (d, J = 7.6 Hz, 2H), 7.80 (d, J = 8.4 Hz, 4H), 7.60 (d, J = 8.0 Hz, 2H), 7.55 (d, J = 7.2 Hz, 2H), 7.38 (t, J = 7.6 Hz, 4H), 7.29 (d, J = 8.0 Hz, 6H), 7.19−7.13 (m, 16H), 7.05 (t, J = 6.8 Hz, 4H), 6.92 (d, J = 7.2 Hz, 2H); ^{13}C NMR ($CDCl_3$, 100 Hz) δ 154.0, 153.9, 149.8, 148.5, 148.0, 147.4, 141.8, 141.4, 137.3, 132.6, 132.3, 130.8, 129.8, 129.5, 129.3, 128.1, 127.9, 127.8, 127.0, 124.8, 124.4, 124.3, 123.3, 122.8, 120.2, 120.0; MS (m/z, FAB^+) 1071.3 (50), 907.1 (100); HRMS calcd for $C_{73}H_{46}N_6S_2$ 1071.3304, found 1071.3308.

Synthesis of Nanoparticles. The reprecipitation method was used for nanoparticle synthesis.[3] Spiro-BTA NPs were synthesized by injecting 100 μL of Spiro-BTA in THF (5×10^{-4} M) into 10 mL of deionized water (or to a 100 mM Triton X-100 aqueous solution when using surfactant) under sonication at room temperature. The resulting NP solution, after filtering through a 0.22 μm pore-sized filter (Millex GP, PES membrane) had a pale yellow color. The particles are stable for 1 week based on DLS measurements.

Instrumentation. UV−vis spectra were recorded on a DU-800 spectrophotometer (Beckman Coulter, Inc., Brea, CA). Fluorescence spectra were recorded on a Fluorolog-3 spectrofluorimeter (ISAJobin Yvon Horiba, Edison, NJ), using a 1 cm path length quartz cuvette, and the samples were excited at their absorption maxima, with a slit width of 50 nm. Scanning electron microscopy (SEM) was performed with a LEO 1450VP microscope at an accelerating voltage of 20 kV and linked with an Oxford Instruments X-ray analysis system. ζ-Potential analysis was carried out with a Zeta Plus (Brookhaven Instruments Corp., Holtsville, NY). Particle size distribution and measurement utilized a 90Plus/BI-MAS (Brookhaven Instruments Corp., Holtsville, NY) instrument.

Electrochemical methods such as multipotential step and cyclic voltammetry (CV) were performed with a conventional three-electrode cell linked to a CH Instruments electrochemical workstation model 660 (Austin, TX). The electrochemical/ECL cell contained an L-type inlaid platinum disk as a working electrode, which was polished with alumina of different sizes between each experiment. The other electrodes were a platinum coiled wire counter electrode and a Ag wire quasireference electrode (for solution electrochemistry and ECL) or, in aqueous solutions, a Ag/AgCl reference electrode (nanoparticle experiments). Current and ECL transients were simultaneously recorded using an

dx.doi.org/10.1021/ja2000825 |J. Am. Chem. Soc. 2011, 133, 5492–5499

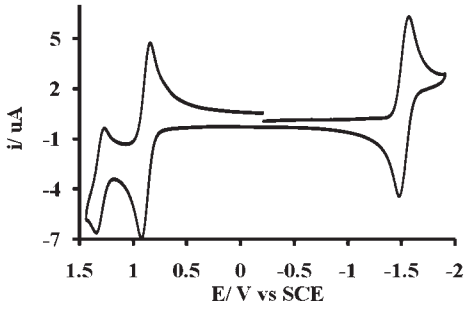

Figure 1. Cyclic voltammogram of ~1 mM Spiro-BTA in Bz:MeCN (2:1): electrolyte, 0.1 M Bu_4NPF_6; scan rate, 100 mV/s; working electrode, ~1 mm Pt disk; counter electrode, platinum coil; reference electrode, Ag wire (calibrated against Fc/Fc^+). Initial scan direction is cathodic.

Autolab electrochemical workstation (Eco Chemie) coupled with a photomultiplier tube (PMT, Hammamatsu R4220p) held at −750 V with a high-voltage power supply (Kepco, Flushing, NY). The photocurrent produced at the PMT was converted to a voltage signal by an electrometer/high-resistance system (Keithley, Cleveland, OH) and fed into the external input channel of an analog-to-digital converter (ADC) of the Autolab. Emission spectra were obtained with a charge coupled device (CCD) camera (Princeton Instruments, SPEC-10) that was cooled to −100 °C. The CCD camera and monochromator wavelengths were calibrated with a mercury lamp prior to each measurement.

To generate ECL via ion annihilation, the working electrode potential was pulsed between the first oxidation and reduction peak potentials with a pulse width of 0.1 s. To generate ECL with a coreactant, the working electrode potential was pulsed between zero and the first oxidation potential of both the coreactant and Spiro-BTA NPs. Digital simulations of cyclic voltammograms were performed with Digisim Software package 3.0 (Bioanalytical Systems, Inc., West Lafayette, IN), to investigate the mechanisms of the electrochemical processes.

Chemicals. Anhydrous acetonitrile (MeCN, 99.8% in a sure-sealed bottle) and anhydrous benzene (Bz, 99.9% in a sure-sealed bottle) were obtained from Aldrich. Tetra-*n*-butylammonium hexafluorophosphate (Bu_4NPF_6) was obtained from Fluka and transferred directly into a helium atmosphere glovebox. Tripropylamine (98%) was obtained from Aldrich.

RESULTS AND DISCUSSION

Synthesis of Spiro-BTA. The titled compound Spiro-BTA, consisting of a spirobifluorene core, two benzothiadiazole moieties, and two triphenlyamines, was synthesized from 4,7-dibromobenzo[1,2,5]thiadiazole and 9,9′-spirobifluorene 2,7-diboronic ester (**1**) through a Suzuki coupling reaction. Scheme 1 depicts the synthetic route of Spiro-BTA from compound **1**. Selective Suzuki coupling of the diboronate **1** with an excess amount (6 equiv) of dibromobenzothiadiazole afforded the dibromo **2**[1c] in 30% yield. The dibromo compound **2** was subjected to coupling with *N*,*N*-diphenyl-4-(4,4,5,5-tetramethyl-1,3,2-dioxaborolan-2-yl)aniline (**3**)[6] in the presence of a catalytic amount of $Pd(PPh_3)_4$ and cocatalyst P^tBu_3 to give Spiro-BTA in 82% yield.

Electrochemistry. Figure 1 shows the cyclic voltammogram (CV) of a 1 mM Spiro-BTA solution in benzene:MeCN (v/v, 2:1)/0.1 M Bu_4NPF_6. The results are summarized in Table 1. The oxidation scan shows two waves, at $E^o_{1,ox}$ = 0.88 V (i_{pa} = 6 μA) and $E^o_{2,ox}$ = 1.30 V (i_{pa} = 3 μA) vs SCE. The peak current of the first wave is twice that of the second, so the first peak is probably composed of two overlapping sequential one-electron transfer reactions, and the second wave also involves a one-electron transfer. From the chemical structure and the groups in the Spiro-BTA, the first oxidation waves can be assigned to the oxidation of the two terminal triphenylamine groups. The two closely spaced waves clearly indicate that there is negligible electronic communication between the two donor groups. The reversibility of these waves, even at a scan rate of 50 mV/s, indicates a high stability of the dication ($D^{+\bullet}$~A~F~A~$D^{+\bullet}$). With ΔE^o = 50 mV between the two reversible 1e oxidations of the triphenylamines and the heterogeneous electron transfer rate constant showing Nernstian behavior, the digital simulation of the oxidation CVs over a broad range of scan rates (50−1000 mV/s) (Figure 2) shows a good fit to the experimental CV, consistent with the assumption of a weak electronic coupling of two terminal donor groups.

The second one-electron transfer oxidation wave is reversible, even at a scan rate of 50 mV/s. This oxidation potential is consistent with that of the central fluorene moiety,[7] which now has extended π-conjugation via 2,7-substitution. Spiro-BTA shows a reduction peak at −1.45 V vs SCE (i_{pc} = 6 μA), which exhibits the same peak height as the first 2e oxidation wave. Therefore, we assigned this to a Nernstian two-electron transfer peak, originating from the sequential reductions of the two acceptor 2,1,3-benzothiadiazole groups. As with the oxidation, digital simulation of the reduction CVs with ΔE^o = 60 mV between the two reversible 1e waves was carried out. The heterogeneous electron transfer rate constant employed in simulated CVs that fit the experimental data best was k^o ~ 0.01 cm/s over scan rates of 50−1000 mV/s (Figure 3). Thus, the reduction of both benzothiadiazole groups at relatively the same potential is also indicative of the lack of electronic communication between the two benzothiadiazoles via the fluorene linkage, but it is slower than the oxidations, perhaps because these A-groups are sterically slightly less accessible than the D-groups. However, the slightly larger ΔE^o ($E^o_{2,red} - E^o_{1,red}$) = 60 mV might also suggest a stronger electrostatic repulsion between the two acceptor groups because of the smaller separation distance as compared to that of the donor groups.[8] Scan rate (v) studies show that the anodic and cathodic currents of the first oxidation and reduction peaks of Spiro-BTA were proportional to $v^{1/2}$. The peak current ratio is approximately unity down to a scan rate of 50 mV/s, indicating the absence of a following chemical reaction. This suggests that the oxidation to a stable radical dication and the reduction to a stable dianion are essentially Nernstian.

Figure 4 depicts the theoretical calculation of optimized ground-state geometry of Spiro-BTA calculated by B3LYP/STO-3G. The dihedral angle between spirobifluorene and 2,1,3-benzothidiazole is 17°, and a twisted conformation between triphenylamine and benzothiadizole with a dihedral angle of 15° is observed. The optimized geometry indicates Spiro-BTA is not coplanar, which may explain the small electronic coupling indicated by the redox processes. This agrees with the experimental and simulation results that conclude the electronic communication between the two donor groups and between the two acceptors via the fluorene bridge is weak.

Spectroscopic Characterization of Spiro-BTA Solutions and NPs. Figure 5 shows the SEM image of fresh Spiro-BTA nanoparticles dispersed in aqueous solution with an average diameter of ~130 nm. Dynamic light scattering (DLS) of the Spiro-BTA NPs solution confirms the observation obtained by

Table 1. Electrochemical (CV) and Spectroscopic Results for Spiro-BTA in Solution (1:2 MeCN:Bz)

$E^{o}_{1,ox}$ (V vs SCE)	$E^{o}_{2,ox}$ (V vs SCE)	$E^{o}_{1,red}$ (V vs SCE)	λ_{max}^{Abs} (nm)	λ_{max}^{FL} (nm)	λ_{max}^{ECL} (nm)	Φ_{PL}	Φ_{PL}^{film}
0.88	1.30	−1.45	450	622	635	0.47	0.51

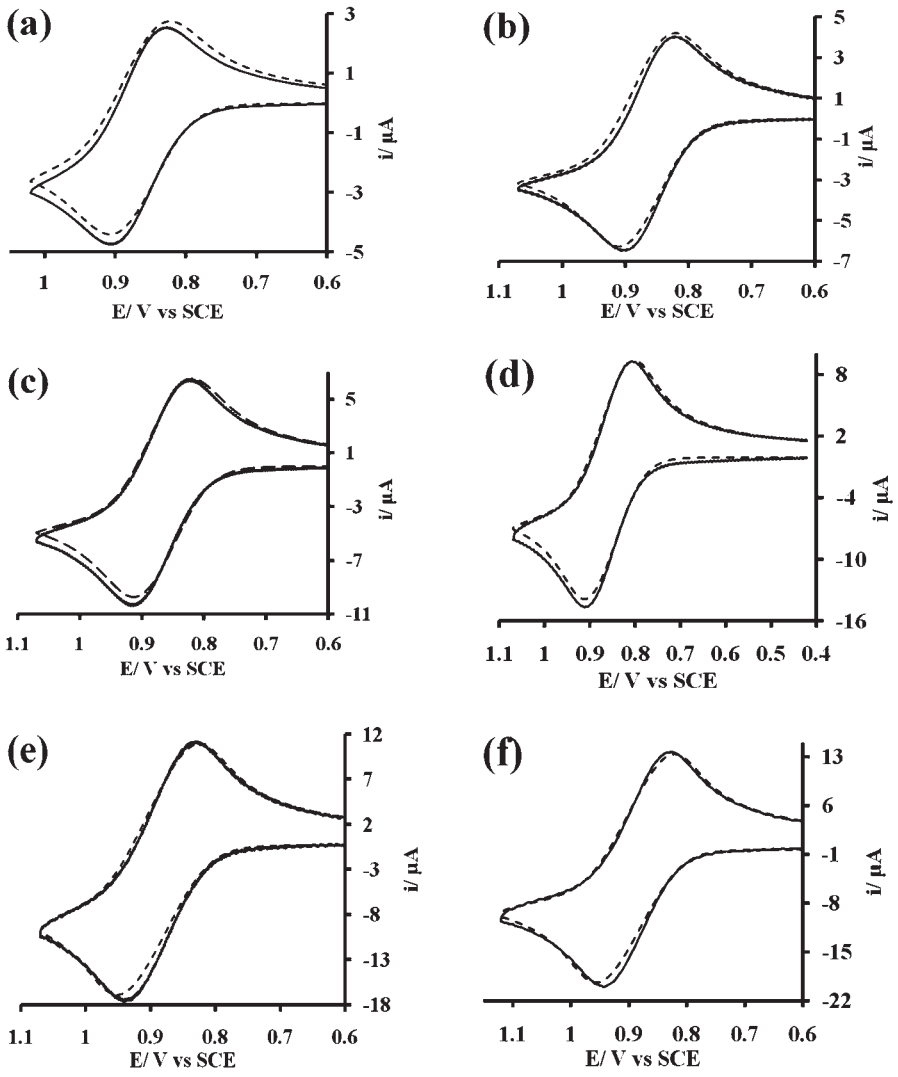

Figure 2. Simulation of ∼1 mM Spiro-BTA oxidation at different scan rates. Simulation parameters involve two one-electron oxidations with D_O = 6.5 × 10^{-6} cm^2/s, $E^{o}_{1,ox}$ = 0.86 V vs SCE, $E^{o}_{2,ox}$ = 0.91 V vs SCE, k^o = 1 × 10^4 cm/s, α = 0.5, uncompensated resistance R_u = 2 KΩ, and double layer capacitance C_d = 50 nF at (a) 0.05 V/s, (b) 0.1 V/s, (c) 0.25 V/s, (d) 0.5 V/s, (e) 0.75 V/s, (f) 1 V/s. Simulation (dotted line), experimental (solid line).

SEM (Supporting Information, Figure S2). The particle size was stable even after 1 week under ambient conditions (in the dark and under sunlight) without adding any surfactant to provide extra stabilization. However, when prepared in the presence of Triton X-100, the Spiro-BTA NPs size decreased to ∼100 nm, and the distribution of particle sizes was more uniform with no aggregation detected by DLS (Supporting Information, Figure S3). The electrochemistry in an aqueous solution of the Spiro-BTA NPs did not show a distinctive redox peak because of the low concentration of the NPs and their small diffusion coefficient.

Absorption and emission spectra of the Spiro-BTA dissolved in a solution of benzene:MeCN 2:1 are shown in Figure 6. The absorption spectrum shows two maxima, one at shorter wavelength (305 nm), which is attributed to the $\pi-\pi^*$ transition of the fluorene,[9] while the other at longer wavelength (445 nm) is ascribed to the $\pi-\pi^*$ transition of Spiro-BTA. Spiro-BTA shows a PL emission maximum centered at 612 nm with a quantum yield of 0.45 in THF solution and 0.51 for a solid film measured by a calibrated integrated sphere. The observed large Stokes shift implies a possible conformational change upon photoexcitation. Since Spiro-BTA is composed of donor and acceptor subunits, emission from a photoexcited intramolecular charge transfer (ICT) can also account for the evident Stokes shift. The solvent-polarity-independent UV−vis absorption spectra of Spiro-BTA as shown in Figure 6c indicate that there is no strong charge transfer in the ground state. However, the PL emission spectra of Spiro-BTA show significant red-shifts from low-polarity to high-polarity solvents along with decreased PL intensity, e.g.,

dx.doi.org/10.1021/ja2000825 |J. Am. Chem. Soc. 2011, 133, 5492–5499

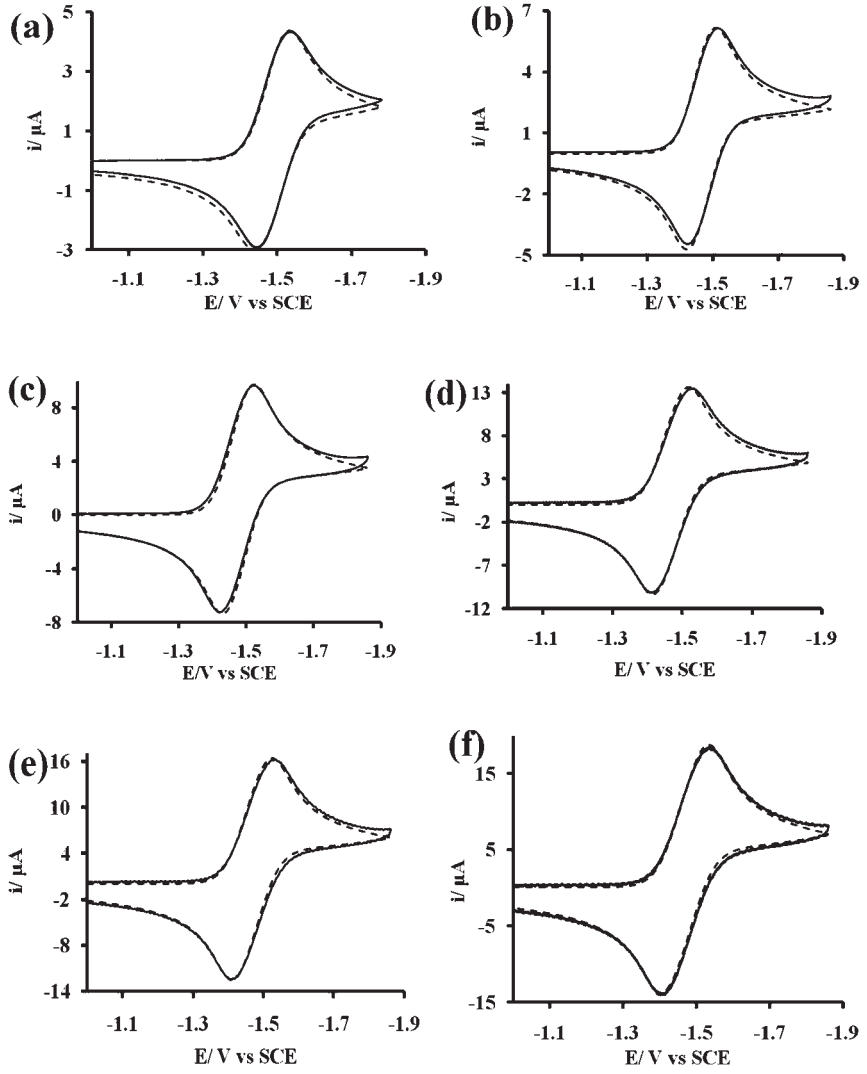

Figure 3. Simulation of ~1 mM Spiro-BTA reduction at different scan rates. Simulation parameters for two one-electron reductions with $D_O = 6.5 \times 10^{-6}$ cm^2/s, $E^o_{1,red} = -1.42$ V vs SCE, $E^o_{2,red} = -1.48$ V vs SCE $k^o = 0.01$ cm/s, $\alpha = 0.5$, $R_u = 2$ KΩ, and $C_d = 50$ nF at scan rates of (a) 0.05 V/s, (b) 0.1 V/s, (c) 0.25 V/s, (d) 0.5 V/s, (e) 0.75 V/s, (f) 1 V/s. Simulation (dotted line), experimental (solid line).

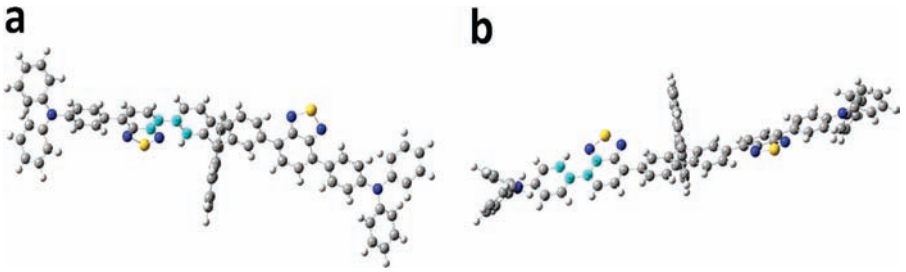

Figure 4. Optimized ground-state geometry calculated by B3LYP/STO-3G: (a) light blue indicates the dihedral angle between the benzothiadiazole and spirobifluorene planes and (b) light blue indicates the dihedral angle between triphenylamine and benzothiadiazole planes.

green emission (537 nm) in cyclohexane to orange-red emission (624 nm) in CH_2Cl_2 (Figure 6b,d). The strong solvent-polarity-dependent PL indicates that that Spiro-BTA has a highly charged excited state due to photoinduced charge transfer.

We prepared three types of samples to study the photophysical properties of Spiro-BTA NPs. Sample A consisted of fresh Spiro-BTA NPs, sample B was NPs with Triton X-100 in water, and sample C was a solution of 100 μL of 1 mM Spiro-BTA in 10 mL of THF. The absorption and emission spectra of Spiro-BTA NPs with and without surfactant (Triton X-100) as compared to that in solution are shown in Figure 7. The absorption maximum of Spiro-BTA in THF solution (sample C) is located at 450 nm, while the absorption maxima are red-shifted by 18 nm (at 468 ± 2 nm) for Spiro-BTA NPs (sample A). The UV−vis spectra of

dx.doi.org/10.1021/ja2000825 |*J. Am. Chem. Soc.* 2011, 133, 5492–5499

Spiro-BTA NPs strongly suggest that Spiro-BTA is not molecularly dissolved but rather well-dispersed as colloidal particles. This UV−vis spectral shift indicates that the particles are self-assembled as aggregates during the recrystallization process.[10] In contrast, the emission of Spiro-BTA NPs colloid solution is blue-shifted by 10 nm as compared to that of Spiro-BTA in THF. More interestingly, the PL intensity of Spiro-BTA NPs is increased over the one in solution, especially in the presence of surfactant (Figure 7b). The blue-shifted emission is due to the restricted conformational relaxation in the NPs, which also leads to the enhancement of emission intensity as reported for aggregation-induced emission enhancement (AIEE).[11] Similar behaviors, such as red-shifted absorption and blue-shifted emission, were observed in a thin solid film of Spiro-BTA (Figure S4, Supporting Information), which was prepared by spin-coating of a 1×10^{-3} M solution (THF) at 1000 rpm.

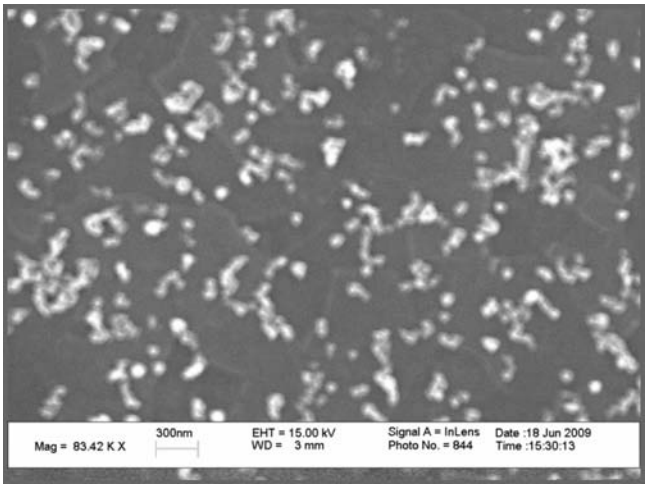

Figure 5. SEM image of organic NPs of Spiro-BTA prepared in water. Scale marker is 300 nm.

Electrogenerated Chemiluminescence (ECL) in Solution. Annihilation ECL was obtained by alternating the potentials of the working electrode from the first oxidation potential (E_p^{ox} = +50 mV) to the first reduction potential (E_p^{red} = −50 mV). Spiro-BTA dissolved in organic solution (Bz:MeCN) produced strong ECL emission that was easily seen with the naked eye in a well-lit room. The ECL spectrum of Spiro-BTA, shown in Figure 8, is characterized by an ECL maximum centered at 635 nm, red-shifted by 13 nm from the fluorescence maximum. Such a red-shift in ECL emission is often encountered in ECL spectra and is attributed to an inner filter effect because of the different concentrations used for PL (μM) and ECL (mM). An additional small factor in the red-shifted ECL peak is that different instruments were used for acquiring the PL and ECL.

The enthalpy of radical ion annihilation (2.23 eV) is calculated as[12] $\Delta H_{ann} = E^o_a - E^o_c - 0.1$, where E^o_a is the anodic formal potential, E^o_c is the cathodic formal potential, and ΔH_{ann} is greater than the energy required to produce the excited state $E_s = 1239$ (λ_{max} nm) (~2 eV). This result indicates that the ECL emission is directly formed via an annihilation reaction to give the singlet excited state, which is also called an energy-sufficient or S-route. Transient ECL (i-t-ECL) depicted in Figure 9 shows that equal ECL intensity is seen upon each anodic to cathodic pulse cycle, indicating that the same amount of cation/dication and anion/dianion are formed upon each pulse. In addition, all radicals and ions are stable within the time scale of the ECL experiment.

ECL of Organic Nanoparticles. Although the electrochemistry of the NPs could not be observed, they did produce ECL upon electrochemical excitation. Because of the limited potential window at negative potentials in aqueous solution, we were limited to seek ECL by oxidation of the NPs. For this reason, we

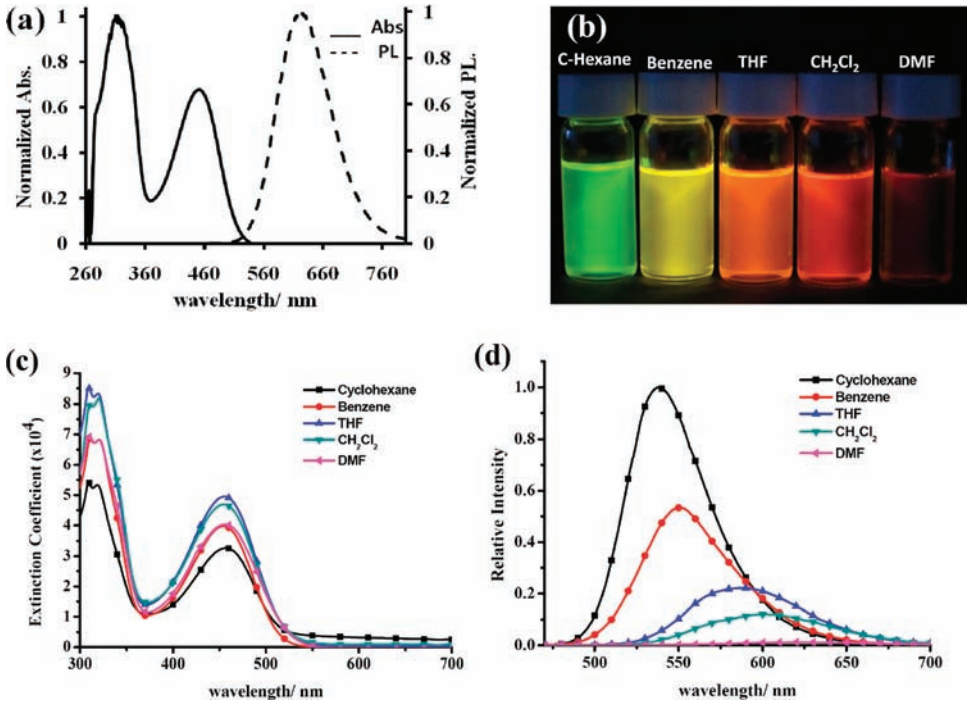

Figure 6. (a) Absorbance (solid line) and fluorescence spectra (dotted line) of Spiro-BTA in a solution of benzene:MeCN 2:1. (b) Emission color of Spiro-BTA in different solvents. (c) Absorption and (d) photoluminescence spectra of 9×10^{-5} M Spiro-BTA in different solvents.

dx.doi.org/10.1021/ja2000825 |J. Am. Chem. Soc. 2011, 133, 5492–5499

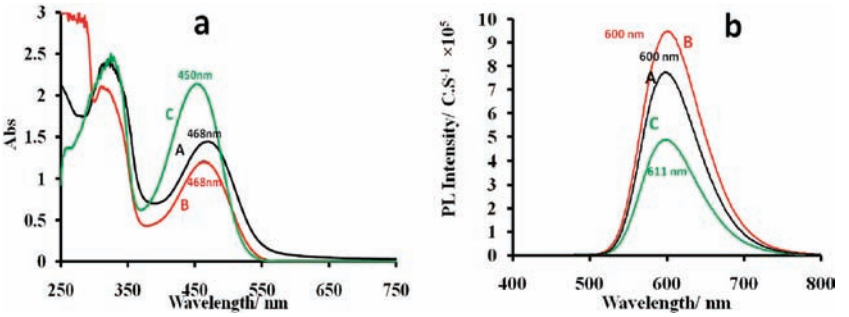

Figure 7. (a) Absorption and (b) emission spectra: (A, black) fresh Spiro-BTA NPs, (B, red) NPs with Triton X-100 in water, and (C, green) 100 μL of 1 mM Spiro-BTA in 10 mL of THF.

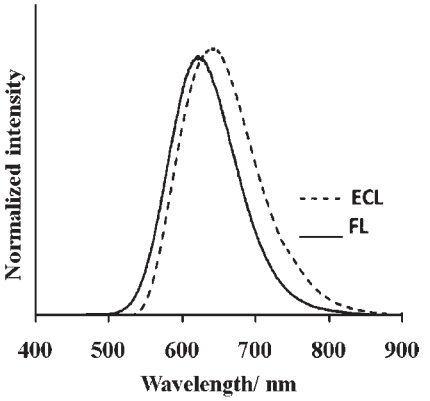

Figure 8. ECL and fluorescence spectra of Spiro-BTA in Bz:MeCN 2:1 solution: ECL integration time, 1 min; slit width, 0.5 mm; pulsing range, E_{pa} = +70 mV to E_{pc} = −70 mV.

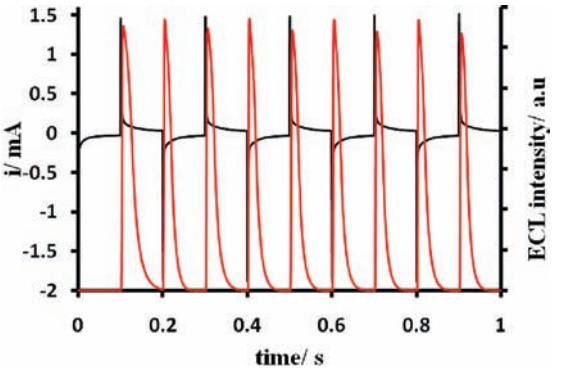

Figure 9. i-t-ECL of ~1 mM Spiro-BTA, pulsing was from E_{pa} = +70 mV to E_{pc} = −70 mV (black line is current, red line is ECL intensity).

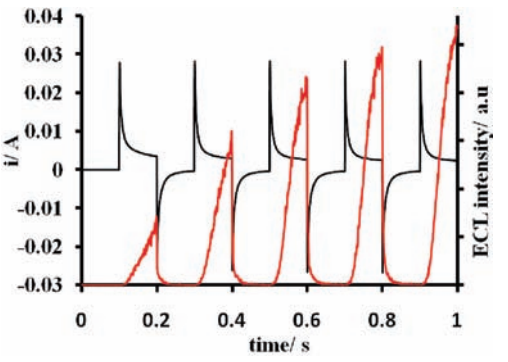

Figure 10. i-t-ECL Spiro-BTA NPs in water with 0.1 M TPrA as a coreactant, pulsing from 0.0 V to +1.2 V vs Ag/AgCl.

used a coreactant that produces a strong reducing agent, tri-*n*-propylamine (TPrAH), a well-known coreactant that oxidizes electrochemically at 0.9 V vs SCE, producing, upon loss of a proton, a strong reducing agent (−1.7 V versus SCE).[13] The ECL from well-dispersed Spiro-BTA NPs in the absence of surfactants in aqueous medium is shown in Figure 10 when the electrogenerated oxidized NPs ($NP^{+\bullet}$) on the surface of the particles reacted with the strong reducing agent ($TPrA^{\bullet}$)

$$NP - e \rightarrow NP^{+\bullet}$$
$$TPrAH - e \rightarrow TPrAH^{+\bullet}$$

$$TPrAH^{+} + NP \rightarrow NP^{+\bullet} + TPrAH$$

$$TPrAH^{+} \rightarrow {}^{\bullet}TPrA^{\bullet} + H^{+-}$$

$$NP^{+\bullet} + TPrA^{\bullet} \rightarrow TPrA^{+\bullet} + NP^{*}$$

$$NP^{*} \rightarrow NP + h\nu$$

There is no evidence of electrode fouling, and the increasing ECL signal on cycling perhaps suggests that adsorption with formation of an emitting film is a possibility. However, the ECL signal was not strong, and although it could be recorded with a photomultiplier tube, it was not sufficiently stable to obtain an ECL spectrum. The relatively weak ECL of Spiro-BTA NPs can be attributed to the small diffusion coefficient of the particles to the electrode surface as well as the instability of the cationic states in the aqueous solution. NPs could adsorb on the surface of the electrode, so electrode fouling is one of the reasons for the weak ECL light.

CONCLUSIONS

A new red-emitter (Spiro-BTA) based on a D−A−π−A−D structure, where D is triphenylamine, A is 2,1,3-benzothiadiazole, and π is spirofluorene, has been synthesized and characterized. The dianion and dication of Spiro-BTA is highly stable upon electrochemical reduction and oxidation, respectively. The absence of D/A charge transfer in the ground state was verified by the solvent-polarity-independent UV−vis absorption spectra of Spiro-BTA, whereas the strongly red-shifted PL in polar solvents

dx.doi.org/10.1021/ja2000825 |*J. Am. Chem. Soc.* 2011, 133, 5492–5499

confirms the charge separation in the excited state. Well-dispersed Spiro-BTA nanoparticles were prepared in aqueous solution using a reprecipitation method. Spiro-BTA has a high quantum yield in solution and even higher as nanoparticles, and as the particles size becomes smaller in the presence of surfactant, the quantum yield becomes higher. ECL of Spiro-BTA in organic solution is intense and can be seen with the naked eye in ambient light. The ECL of Spiro-BTA NPs can be observed with the aid of TPrA as a coreactant by the oxidation of both coreactant and nanoparticles simultaneously. As with inorganic NPs, organic nanoparticle ECL as emissive tags for bioanalytical applications in aqueous solution would be of interest, if the intensities could be improved.

■ ASSOCIATED CONTENT

Supporting Information. Detailed synthetic procedure and spectroscopic characterization of Spiro-BTA, DLS measurements for Spiro-BTA NPs, absorption and photoluminescence spectra of Spiro-BTA thin film, and a Lippert plot. This material is available free of charge via the Internet at http://pubs.acs.org.

■ AUTHOR INFORMATION

Corresponding Authors
ajbard@mail.utexas.edu; kenwong@ntu.edu.tw

■ ACKNOWLEDGMENT

This work was financially supported by the National Science Foundation (CHE-0808927), the Robert A. Welch Foundation (F-0021), Roche Diagnostics, Inc., and the National Science Council, Taiwan.

■ REFERENCES

(1) (a) Fungo, F.; Wong, K.-T.; Ku, S.-Y.; Hung, Y.-Y.; Bard, A. J. *J. Phys. Chem. B* **2005**, *109*, 3984. (b) Rashidnadimi, S.; Hung, T. H.; Wong, K.-T.; Bard, A. J. *J. Am. Chem. Soc.* **2008**, *130*, 634. (c) Omer, K. M.; Ku, S.-Y.; Wong, K.-T.; Bard, A. J. *J. Am. Chem. Soc.* **2009**, *131*, 10733. (d) Omer, K. M.; Ku, S.-Y.; Wong, K.-T.; Bard, A. J. *Angew. Chem., Int. Ed.* **2009**, *48*, 9300. (e) Shen, M.; Rodríguez-López, J.; Lee, Y.-T.; Chen, C.-T.; Fan, F.-R. F.; Bard, A. J. *J. Phys. Chem. C* **2010**, *114*, 9772. (f) Omer, K. M.; Ku, S.-Y.; Chen, Y.-C.; Wong, K.-T.; Bard, A. J. *J. Am. Chem. Soc.* **2010**, *132*, 10944.

(2) Asahi, T.; Sugiyama, T.; Masuhara, H. *Acc. Chem. Res.* **2008**, *41*, 1790.

(3) (a) Kasai, H.; Nalwa, H. S.; Oikawa, H.; Okada, S.; Matsuda, H.; Minami, N.; Kakuta, A.; Ono, K.; Mukoh, A.; Nakanishi, H. *Jpn. J. Appl. Phys.* **1992**, *31*, 1132. (b) Kasai, H.; Oikawa, H.; Okada, S.; Nakanishi, H. *Bull. Chem. Soc. Jpn.* **1998**, *7*, 2597. (c) Horn, D.; Rieger, J. *Angew. Chem., Int. Ed.* **2001**, *40*, 4330. (d) Fu, H. B.; Xiao, D. B.; Yao, J. N.; Yang, G. Q. *Angew. Chem., Int. Ed.* **2003**, *42*, 2883. (e) Hu, J. S.; Guo, Y. G.; Liang, H. P.; Wan, L. J.; Jiang, L. *J. Am. Chem. Soc.* **2005**, *127*, 17090. (f) Zhang, X. J.; Zhang, X. H.; Shi, W. S.; Meng, X. M.; Lee, C. S.; Lee, S. T. *Angew. Chem., Int. Ed.* **2007**, *46*, 1525.

(4) Omer, K. M.; Bard, A. J. *J. Phys. Chem. C* **2009**, *113*, 11575.

(5) Yu, J.; Fan, F.-R. F.; Pan, S.; Lynch, V. M.; Omer, K. M.; Bard, A. J. *J. Am. Chem. Soc.* **2008**, *130*, 7196.

(6) Medina, A.; Claessen, C. G.; Rahman, G. M. A.; Lamsabhi, A. M.; Mo, O.; Yanez, M.; Guldi, D. M.; Torres, T. *Chem. Commun.* **2008**, 1759.

(7) Fungo, F.; Wong, K.-T.; Ku, S.-Y.; Hung, Y.-Y.; Bard, A. J. *J. Phys. Chem. B* **2005**, *109*, 3984.

(8) Bard, A. J.; Faulkner, L. R. *Electrochemistry: Fundamentals and Applications*; John Wiley & Sons: New York, 2001; p 246.

(9) Kalsi, P. S. *Spectroscopy of Organic Compounds*, 6th ed.; New Age International Ltd.: New Delhi, 2004; pp 13.

(10) (a) Tomioka, A.; Anzai, T.; Kamiyama, Y. *e-J. Surf. Sci. Nanotechnol.* **2009**, *14*, 89. (b) Kitahama, Y.; Takazawa, K. *Bull. Chem. Soc. Jpn.* **2008**, *81*, 1282.

(11) (a) Deans, R.; Kim, J.; Machacek, M. R.; Swager, T. *J. Am. Chem. Soc.* **2000**, *122*, 8565. (b) Zeng, Q.; Li, Z.; Dong, Y.; Di, C.; Qin, A.; Hong, Y.; Ji, L.; Zhu, Z.; Jim, K. W.; Yu, G.; Li, Q.; Li, Z.; Liu, Y.; Qin, J.; Tang, B.-Z. *Chem. Commun.* **2007**, 70.

(12) Bard, A. J. *Electrogenerated Chemiluminescence*; Marcel Dekker: New York, 2004; p 8.

(13) Lai, R. Y.; Bard, A. J. *J. Phys. Chem. A* **2003**, *107*, 3335.